

Characterisation of an all-optical inverse Compton scattering source for industrial imaging

Contact: c.mcanespie@qub.ac.uk

C.A. McAnespie, M.J.V. Streeter, L. Calvin, N. Cavanagh, K. Fleck, G. Sarri
School of Mathematics and Physics, Queen's University Belfast, BT7 1NN, Belfast, UK.

B. Kettle
The John Adams Institute for Accelerator Science, Imperial College London, London, SW7 2AZ, UK.

W. Sun
National Physical Laboratory, Hampton Road, Teddington, TW11 0LW, UK.

Abstract

We report on the production of an all-optical inverse Compton scattering (ICS) source for industrial imaging generated using a two-laser configuration. Successful laser-electron ICS interactions were obtained for electron energies up to ~ 1 GeV, with numerical estimates suggesting photon energies in the range of approximately 1-10 MeV were achieved. The duration of the photon bunch can be estimated as < 50 fs with a source size on the order of $10 \mu\text{m}$. Imaging of reference line pairs was used to demonstrate a resolution of $170 \mu\text{m}$, highlighting the unique advantages of this source.

1 Introduction

Inverse Compton scattering based on colliding an energetic electron beam with an intense laser pulse has the ability to generate high flux, low divergence, energy-tunable photon bunches with ultra-short duration [1, 2]. ICS photon sources have been developed with conventional accelerators, however their large size and cost has limited their development to the generation of MeV-scale photon sources. Recent advances in laser wakefield accelerators (LWFA) have resulted in the generation of high brightness electron sources capable of producing MeV-scale photons through ICS in compact set-ups [2, 3, 4, 5]. Furthermore, the size of these electron beams at the exit of the LWFA accelerator infers that the source size of an ICS photon source is typically on the order of $10 \mu\text{m}$, allowing for high resolution imaging.

Current work on ICS sources for imaging have been mostly limited to a single laser set-up, where the LWFA laser is reflected using a plasma mirror [4, 6, 7]. Some work has been performed in the two laser configuration [5, 8, 9] with test radiographs performed [10]. While these single-beam sources are effective and easier to implement, the reflected laser parameters are difficult

O. Finlay, K. Fedorov, C.D. Armstrong, S.J.D. Dann, B. Spiers, D.R. Symes
Central Laser Facility, STFC Rutherford Appleton Laboratory, Didcot, OX11 0QX, UK.

J.M. Warnett, E. Kiely
WMG, University of Warwick, Coventry, CV4 7AL, UK.

to control (typical durations < 45 fs and normalised intensities (a_0) of 1-2). This is particularly important when considering the flux of the scattered photon source, which is proportional to the duration of the number of optical periods (N_{opt}) in the scattering laser at constant intensity ($N_\gamma \propto N_{opt} a_0^2$ for $a_0 < 1$ [1]). Although more challenging in terms of spatial and temporal alignment, the use of an independently controllable scattering laser is beneficial for optimising and controlling the ICS photon source.

2 Experiment set-up

The experiment was performed using the Gemini laser at the Central Laser Facility (CLF). A sketch of the geometry is shown in figure 1. The laser-wakefield was driven by the South beam delivering 6.7 ± 0.3 J of energy in 45 ± 5 fs FWHM duration. The laser was focused using an F/40 off-axis parabolic mirror (OAP) producing a normalised laser intensity of $a_0 = 1.6 \pm 0.1$.

A 15 mm conical nozzle was used to produce a supersonic gas jet with a mixed gas target of 2% nitrogen and 98% helium. The North beam acted as the scattering laser for the ICS source, delivering 2.4 ± 0.2 J in 500 ± 40 fs FWHM duration [11]. This scattering laser was focused 5 mm from the exit of the gas jet using an F/7 OAP producing a normalised intensity of $a_0 = 0.55 \pm 0.10$. The scattering laser was folded on-axis with a holed mirror for free propagation of the electrons and scattered photons and to avoid back-reflections into the laser chain.

A permanent magnet dipole was used to sweep the electron beam off-axis for diagnosis by a LANEX scintillator screen. The ICS photon beam was used to illuminate samples at two positions providing a magnification of 1.75 and ~ 1 (Pos. 1 and 2 in figure 1 respectively). The source was imaged by an 8 mm thick LYSO screen 3.7 m from its point of generation. The scintillator was chosen to balance image resolution and signal,

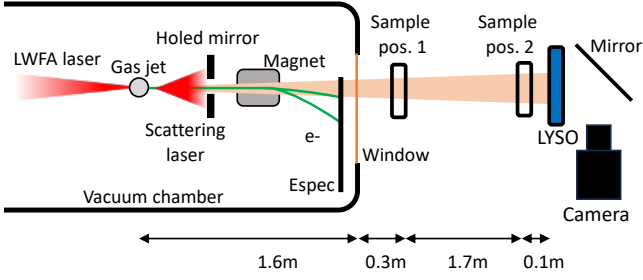


Figure 1: Simplified sketch of the experimental set-up. The South laser was focused with an F/40 OAP onto the gas jet to drive the wakefield accelerator. The North laser was focused on-axis using a holed mirror to produce the inverse Compton photon beam. Samples were imaged downstream of the beam using a LYSO scintillator screen.

with thicker scintillators providing a greater signal at a reduced resolution [12].

3 Source characterisation

Before the source was characterised significant time was spent ensuring good temporal overlap of the electron beam and scattering laser. Inherent jitter of both lasers resulted in significant spatial misalignment of the electron beam and scattering laser, resulting in $\sim 11\%$ of shots producing a usable photon beam for imaging after optimisation.

During source characterisation, the scattering laser

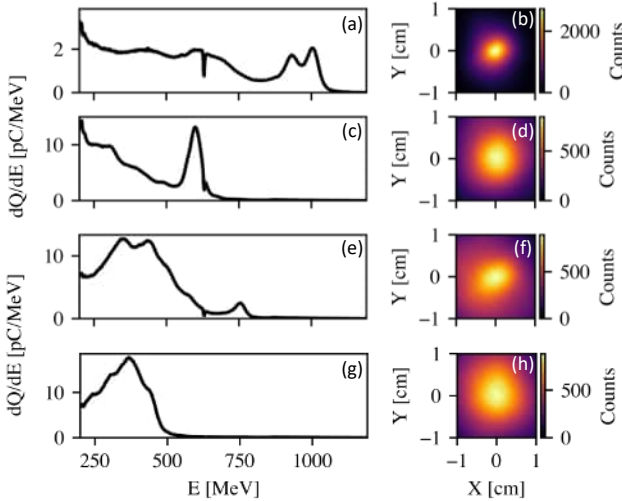


Figure 2: Example electron spectra for increasing electron densities of $2.4\text{--}3.2 \times 10^{18} \text{ cm}^{-3}$ (a,c,e,g) and their respective scattered photon profiles (b,d,f,h) measured on the LYSO screen.

was fixed (500 ± 40 fs FWHM, $a_0 = 0.55 \pm 0.10$) and the electron beam was tuned by altering the electron density. The measured electron and photon properties are displayed in table 1. An example electron spectra and scattered photon profile from each electron density investigated are shown in figure 2. It can be seen that at higher electron densities the mean electron energy decreases while photon divergence increases. This is expected due to the energy dependent divergence of ICS photons ($\theta \approx 1/\gamma$) [1]. Moreover, as the electron density increases, the electron beam charge also rises, leading to an increase in the integrated counts on the LYSO screen ($N_\gamma \propto N_e$). The electron density used for imaging was chosen as $2.9 \pm 0.1 \times 10^{18} \text{ cm}^{-3}$ as it provided the best balance between divergence, photon flux and stability.

While it was not measured during this experiment, the duration of the electron bunch under these conditions can be estimated to be < 50 fs [13]. When ICS is generated with ultra-relativistic electrons, the photon bunch duration can be estimated to equal that of the electron bunch. As the ICS interaction here occurs in the linear regime ($a_0 < 1$), the maximum photon energy can be estimated as $4\gamma^2 E_i$, where γ is the electrons lorentz factor and E_i is the initial photon energy (1.55 eV) [2]. For example, in this set-up, an electron with an energy ≈ 200 MeV will generate a broad photon spectra with a maximum energy ~ 1 MeV.

4 Image quality

The imaging capabilities of the photon source were quantified by illuminating a 5 mm thick tungsten resolution grid. The resulting projection was measured on a 8 mm thick LYSO scintillator screen and imaged with a CCD. The resolution grid was placed 1.9 m (Pos. 1 in fig. 1) from the ICS source while the detector was 3.3 m from the source resulting in a magnification of ~ 1.75 . An example projection illuminating the 400 μm line-pair region of interest is shown in figure 3(a).

The image resolution at this magnification was mea-

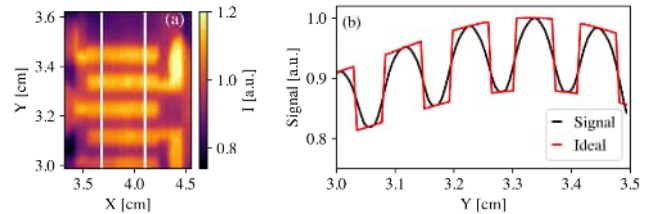


Figure 3: (a): Single shot projection of the resolution grid taken with a magnification of 1.75. The dark and light features highlighted between the two white lines are 400 μm line pairs. (b) The signal (black) averaged between the white banded region of (a). An ideal projection with infinite resolution and zero source size is given in red.

$n_e \times 10^{18} [\text{cm}^{-3}]$	Charge [nC]	σ_e [mrad]	E_{max} [MeV]	σ_γ [mrad]	Int. counts $[\times 10^7]$
2.4 ± 0.1	0.5 ± 0.2	1.82 ± 0.13	760 ± 120	1.3 ± 0.3	4.6 ± 1.7
2.7 ± 0.1	0.9 ± 0.2	1.93 ± 0.20	650 ± 50	1.9 ± 0.5	6.3 ± 3.3
2.9 ± 0.1	1.4 ± 0.3	1.96 ± 0.30	630 ± 30	2.8 ± 0.4	7.7 ± 1.7
3.2 ± 0.1	1.3 ± 0.3	2.12 ± 0.22	560 ± 30	3.3 ± 0.7	8.4 ± 6.4

Table 1: Summary of electron and photon properties over the investigated range of electron densities (n_e). The electron divergence (σ_e) is measured in the non-dispersive direction for $E_e > 200$ MeV. The photon divergence (σ_γ) is quoted as the average of the X and Y divergence ($N > 9$).

sured as $173 \pm 3 \mu\text{m}$, recorded at the central 3 peaks of figure 3(b). The contrast was calculated in terms of peak pixel values and defined as $C = (I_{\text{max}} - I_{\text{min}})/(I_{\text{max}} + I_{\text{min}})$ [12]. For the line-out shown in fig 3(b), the average contrast over the central 3 peaks was measured as $6.8 \pm 1\%$.

5 Sample imaging and CT reconstruction

The imaging capabilities of the source were assessed using a copper tomography test object provided by the National Physical Laboratory (NPL). The object was placed 3.6 m from the source (Pos. 2 in fig. 2, $M \sim 1$) and imaged at multiple angles from 0 to 180 degrees using the golden ratio scanning technique [14, 15]. This angle selection method allows the scan to be terminated at any time, while still retaining a usable data-set. The same gas density was used as in the image quality measurements with the sample moved further from the source to allow for illumination of the whole region of interest. An example, unprocessed, projection taken at an angle of 0 and 90 degrees is shown below in figure 4(a) and (b) respectively.

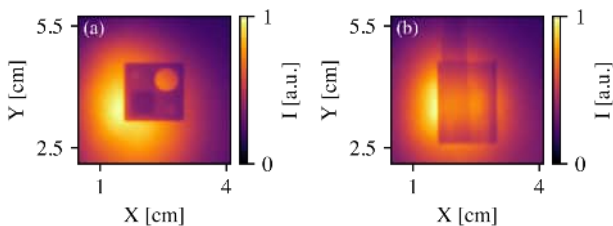


Figure 4: (a) Raw projection at 0 degrees. (b) Raw projection at 90 degrees. A filter has been used to remove hot pixels from hard x-ray hits.

Due to space constraints, the maximum achievable distance from the source was 3.7 m. Consequently, when the sample was rotated 90 degrees, as shown in figure 4(b), the entire sample was not fully or optimally illuminated, given its total length of 3.2 cm. In figure 4(a), the contrast for the thickest (3.2 cm) portion of the sample was measured as $44 \pm 3\%$. The test radiographs here are limited by the pointing fluctuation of the scattered pho-

ton beam, which, in some cases, resulted in only part of the sample being illuminated. As previously mentioned, these pointing fluctuations are inherent to the system and constitute a limitation of the laser system, rather than a limitation of the source.

The capability of this source to produce a computed tomography (CT) of the copper object was tested. This was performed over 147 angles (set by the golden ratio technique) and accumulated over a total number of 1344 shots (450 mins at continuous operation). At each angle position at-least 2 successful projections were taken to account for the pointing fluctuations and ensure maximum illumination of the sample. A successful projection was defined as illuminating the majority of the sample and generating a peak scintillator count that met a user-defined threshold ($\gtrsim 4 \times$ background level). The reconstructed object is shown below in figure 5.

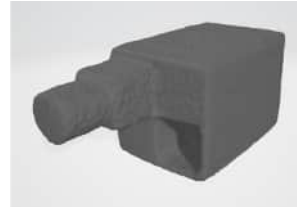


Figure 5: CT reconstruction of the copper object.

It can be seen that the reconstruction provides a good representation of the large object features. However, smaller features are not visible, including the 2 mm diameter, recessed circular features in the top left and bottom right seen in the object in figure 4(a). At this magnification, the image resolution is expected to be $\sim 300 \mu\text{m}$. In this 2 mm cylindrical region of figure 4(a), the contrast is approximately 3.5%. This would suggest that the contrast is the limiting factor in the reconstruction of these smaller embedded features. This could be improved by optimising the detector for increased contrast [12].

6 Conclusions and outlook

An all-optical ICS source was developed, characterised, and utilised to produce radiographs with a resolution of $\sim 170 \mu\text{m}$, limited by the thick LYSO scintillator detector used. The duration of these photon bunches is

estimated as <50 fs, allowing for high resolution images of objects in fast motion. The source size of the photon beam can be estimated as <10 μm , highlighting that with optimisation of the detector the image resolution could be greatly increased. With the limited source-sample distance available, it was demonstrated that this ICS source was capable of producing high quality radiographs with the application to producing a CT reconstruction. Future experiments could focus on optimising the scattering laser beam-line to allow for greater control of the collision parameters and further optimisation of the source. New state-of-the-art facilities, such as EPAC at the CLF, aim to provide improved pointing stability at a higher repetition rate. It can then be envisioned that high-resolution CT could be obtained within a few minutes using an all-optical ICS source produced using EPAC.

7 Acknowledgement

The contribution to this experiment from the National Physical Laboratory was originated from the project *Extending X-ray computed tomography to large and dense components*, which was funded by NPL's Explorer Awards.

References

- [1] Sébastien Corde et al. Femtosecond x rays from laser-plasma accelerators. *Reviews of Modern Physics* **85**, 1 (2013), p. 1.
- [2] Wenchao Yan et al. High-order multiphoton Thomson scattering. *Nature Photonics* **11**, 8 (2017), pp. 514–520.
- [3] S Chen et al. MeV-energy X rays from inverse Compton scattering with laser-wakefield accelerated electrons. *Physical review letters* **110**, 15 (2013), p. 155003.
- [4] K Ta Phuoc et al. All-optical Compton gamma-ray source. *Nature Photonics* **6**, 5 (2012), pp. 308–311.
- [5] Gianluca Sarri et al. Ultrahigh brilliance multi-MeV γ -ray beams from nonlinear relativistic Thomson scattering. *Physical review letters* **113**, 22 (2014), p. 224801.
- [6] Andreas Döpp et al. An all-optical Compton source for single-exposure x-ray imaging. *Plasma Physics and Controlled Fusion* **58**, 3 (2016), p. 034005.
- [7] Yue Ma et al. Region-of-interest micro-focus computed tomography based on an all-optical inverse Compton scattering source. *Matter and Radiation at Extremes* **5**, 6 (2020).
- [8] Nathan D Powers et al. Quasi-monoenergetic and tunable X-rays from a laser-driven Compton light source. *Nature Photonics* **8**, 1 (2014), pp. 28–31.
- [9] Sudeep Banerjee et al. Compact source of narrowband and tunable X-rays for radiography. *Nuclear Instruments and Methods in Physics Research Section B: Beam Interactions with Materials and Atoms* **350**, (2015), pp. 106–111.
- [10] Shouyuan Chen et al. Shielded radiography with a laser-driven MeV-energy X-ray source. *Nuclear Instruments and Methods in Physics Research Section B: Beam Interactions with Materials and Atoms* **366**, (2016), pp. 217–223.
- [11] CA McAnespie et al. High-dose femtosecond-scale gamma-ray beams for radiobiological applications. *Physics in Medicine & Biology* **67**, 8 (2022), p. 085010.
- [12] CID Underwood et al. Development of control mechanisms for a laser wakefield accelerator-driven bremsstrahlung x-ray source for advanced radiographic imaging. *Plasma Physics and Controlled Fusion* **62**, 12 (2020), p. 124002.
- [13] Alexander George Roy Thomas. Scalings for radiation from plasma bubbles. *Physics of Plasmas* **17**, 5 (2010).
- [14] Thomas Kohler. “A projection access scheme for iterative reconstruction based on the golden section”. *IEEE Symposium Conference Record Nuclear Science 2004*. Vol. 6. IEEE. 2004, pp. 3961–3965.
- [15] S. J. D. Dann et al. Computer Tomography with Laser-generated X-rays at Gemini. *CLF Annual Report (2019/20)*.